


Fluid mixing by an electromagnetically driven floating rotorSaúl Piedra *CONACYT-Centro de Ingeniería y Desarrollo Industrial, Querétaro De Arteaga, 76125, Mexico*

Josue Flores

*Instituto de Investigación en Ciencias Básicas y Aplicadas, Universidad Autónoma del Estado de Morelos,
Av. Universidad 1001, Chamilpa, 62209, Cuernavaca, Morelos, Mexico*Guillermo Ramírez *Universidad Tecnológica Emiliano Zapata del Estado de Morelos,
Av. Universidad Tecnológica 1, Palo Escrito, 62765, Emiliano Zapata, Morelos, Mexico*Aldo Figueroa **CONACYT-Centro de Investigación en Ciencias, Universidad Autónoma del Estado de Morelos,
Av. Universidad 1001, Chamilpa, 62209, Cuernavaca, Morelos, Mexico
and Institut de Recherche sur la Biologie de l'Insecte, Université de Tours, Parc de Grandmont, 37200, Tours, France*

Miguel Piñeirua

*Institut de Recherche sur la Biologie de l'Insecte, Université de Tours, Parc de Grandmont, 37200, Tours, France*Sergio Cuevas *Instituto de Energías Renovables, Universidad Nacional Autónoma de México, Temixco, Morelos, 62580, Mexico*

(Received 1 February 2023; accepted 14 July 2023; published 11 August 2023)

We analyze the mixing properties of a floating stirrer driven electromagnetically in a thin layer of electrolyte, consisting of two free-floating magnets with opposite polarities connected by a rigid coupling. The magnetic rotor is set in circular motion using Lorentz forces created due to the interaction of the magnetic field of the rotor with dc currents actuated in logic sequence. We identify a coherent structure similar to a tripolar vortex whose central vortex rotates in the same direction of the rotor promoting chaotic mixing of the fluid in the laminar regime ($Re = 45$). Dyed water visualization and particle image velocimetry were performed to characterize experimentally the mixing and flow dynamics at the surface of the electrolyte layer. A quasitwo-dimensional numerical simulation based on the immersed boundary method, which incorporates the fluid-solid interaction and reproduces the experimental observations satisfactorily, was carried out. Optimal mixing conditions are determined through the exponential growth of the material interfaces, which are established mainly by varying the distance separating the magnets of the rotor.

DOI: [10.1103/PhysRevE.108.025101](https://doi.org/10.1103/PhysRevE.108.025101)**I. INTRODUCTION**

Coherent structures have long been recognized as playing a fundamental role in the dynamics of rotating two-dimensional flows. Dating back to the 1980s, tripolar vortices were included in the group of basic coherent flow structures of geophysical fluid dynamics, along with monopoles and dipoles [1,2]. A tripolar vortex consists of a central vorticity patch with an elliptical shape and two satellite vortices with opposite vorticity sign to that of the central vortex. The whole structure rotates in the same direction as the core vortex and has nonzero angular momentum. Originally, tripoles were observed in numerical simulations in a variety of ways, arising

spontaneously from an unstable monopolar vortex [3], from a randomly-initialized two-dimensional turbulent flow field [4], by a collision of two misaligned dipolar vortices [5], or from a stable Gaussian vortex with a large quadrupolar perturbation [6]. Laboratory experiments confirmed their existence and showed that they may appear in a homogeneous rotating fluid as a result of unstable cyclonic vortices [7], although they were also found in a linearly stratified fluid [8]. As a matter of fact, at geophysical scale, the formation of large anticyclonic vortices that eventually acquire a tripolar structure was reported in the bay of Biscay [9].

Although attention has been mainly focused on the formation, stability, and dynamic behavior of tripoles, since the understanding of the fundamental processes of efficient mixing is a goal pursued for multiple applications, their transport properties have also been explored. A quasiperiodic motion

* alfil@uaem.mx

was observed in tripoles generated off-axis, which led to continuous stretching and folding of fluid in internal regions of the tripole and the chaotic motion of particles [10]. An extensive numerical study of the transport of a passive scalar due to an advection-diffusion process in a tripolar vortex was performed by Ferreira de Sousa and Pereira [11]. Using both Eulerian and Lagrangian methods, the authors found that transport is suppressed in regular flow regions that constitute the vorticity poles, and instead found that this process mainly occurs in chaotic flow regions that surround the tripolar vortex after its formation.

The dipole vortex can be easily created by a fixed dipolar magnet interacting with an applied electric dc current [12]. Multipolar structures of greater complexity can be achieved by using arrays of magnets [13]. In fact, the use of electromagnetic forces in electrically conducting fluids has played an important role in the search of improving mixing mechanisms [14,15]. Using the approach from [16], where a moving vortex dipole is generated by an electric current and a floating magnet, in this paper we show that a magnetic rotor in circular motion driven by Lorentz forces is able to produce a tripolar vortex in a thin layer of electrolyte in the laminar regime. Although three-dimensional effects may appear in these flows, the present experiments were carried out under conditions where a quasitwo-dimensional behavior prevails. Additionally, using Lagrangian tracking to estimate the growth rates of material interface, we investigate the mixing produced by the flow structure and find the optimal distance separating the magnets of the rotor. We start with the explanation of the experimental and numerical procedure in Secs. II and III, respectively. The results are presented and analyzed in Sec. IV, followed by the concluding remarks in Sec. V.

II. EXPERIMENTAL SET UP

The experimental device consists of a square Plexiglas container with a length of 18 cm, see Fig. 1. The container is partially filled with an electrolytic solution of potassium chloride (KCl) at 20% by weight, with a layer thickness of 0.5 cm so that the total volume of liquid is 162 cm³. The mass density, kinematic viscosity, and electrical conductivity of the electrolyte are $\rho_f = 1.09 \times 10^3$ Kg/m³, $\nu_f = 10^{-6}$ m²/s, and $\sigma = 30.9$ S/m, respectively [13]. A system of two magnets, herein referred to as the rotor, with opposite polarity is mechanically linked with a plastic coupling of length $l = 2.75$ cm. The system was kept afloat at the surface of the electrolyte layer by placing each magnet on a circular plastic film of 1.5 cm diameter and 1.7 mm height. The magnets are made of neodymium-iron-boron alloy, with cylindrical geometry, 5 mm diameter and 2 mm height, and a maximum magnetic field strength of 0.16 T. The mass of the solid (magnet-plastic film system) was measured experimentally with a digital balance, $m_s = 0.25$ g. Additionally, the density of the solid can be calculated by considering the volumes of the magnet and the plastic film as individual cylinders, obtaining $\rho_s = 730$ Kg/m³, which is less dense than water. Due to the weight of each magnet, including the plastic film, the dimple created on the surface is only 0.3 mm deep (approximately 5% of the fluid layer thickness), therefore surface deformation has a negligible effect on the flow dynamics. Similar to [15],

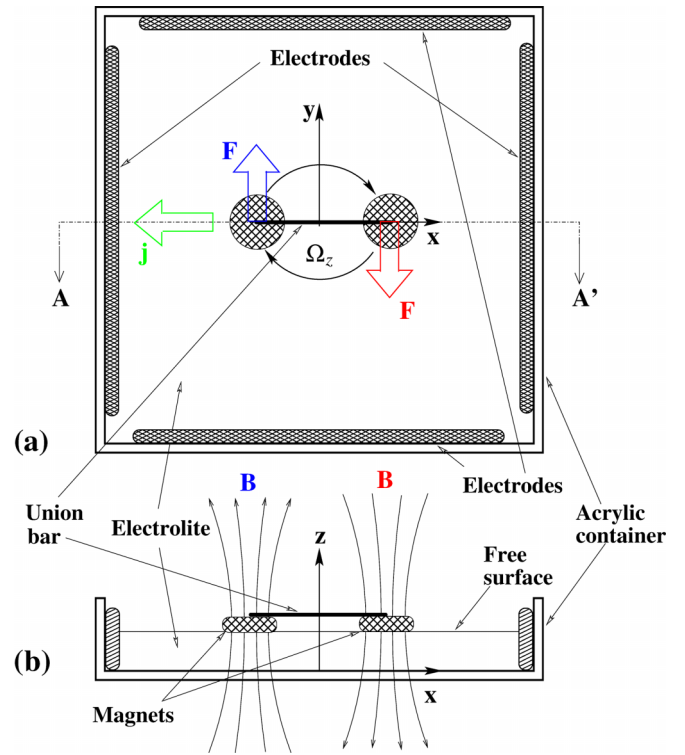


FIG. 1. Sketch of the experimental device, not drawn to scale. Upper panel: plan view. Lower panel: lateral view. The magnetic field \mathbf{B} is generated by a system of mechanically coupled permanent magnets floating on the surface of the fluid layer. The electric current density \mathbf{j} is injected through two pairs of copper electrodes. The main direction of the Lorentz force is denoted by \mathbf{F} .

four electrodes were placed along the sides of the container, connected to a Pololu VNH5019 driver, as a power circuit, controlled by an Arduino UNO REV3, which provided the correct sequence of the applied electric current i to rotate the system of magnets, see Fig. 2. The electric current density is defined as $j = i/A$, where A is the transversal area of the fluid layer. We examined several cases of applied current in the range $200 \leq i \leq 1000$ mA and explored different time duration of electric pulses. However, the rotation of the system was only present for current pulses lasting 4 s at an amplitude

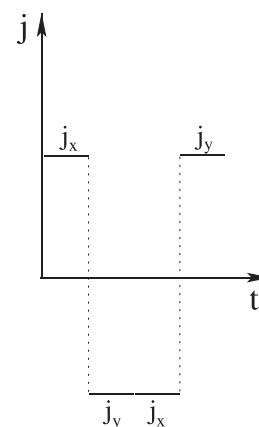


FIG. 2. Diagram of the electric current sequence.

of 700 mA. In the experiments reported in this manuscript, the frequencies of the pulses and applied electric currents used show no effect of electrolysis on the flow of interest. The interaction of the electric current with the localized magnetic fields generates the Lorentz forces in opposite directions that produce a torque which imparts the system an angular velocity Ω_z . Since the floating rotor is very sensitive to other magnetic sources and ferromagnetic materials, the experiments were carried out in an isolated room. The flow was visualized using blue and red vegetable inks poured at the surface. The initial molarity concentration of the dye is $c_0 \approx 10^{-5}$ mol l $^{-1}$. The dyes present a molecular diffusivity $D_m \approx 1 \times 10^{-10}$ m 2 /s and stay at the free surface due to weak thermal effects and follow the motion of the fluid [13]. The dyes are illuminated in volume using two symmetrically located lamps. The lamps are far enough to create a variation of light between the center and the side of the image smaller than 9%. Since the electrolyte is a transparent medium, the bottom wall was covered with a white sheet to ensure the contrast in the visualization. The dynamics of the system was recorded at 24 fps with a high-definition Nikon D84 with a resolution of 1920×1080 pixels. The measurements of the velocity field were obtained with particle image velocimetry (PIV). Spherical hollow glass particles (10 μ m diameter) were seeded to the free surface of the electrolyte layer and illuminated using LEDs. The recorded images were analyzed using PIVLab [17].

III. MATHEMATICAL MODEL

The mathematical model implemented for simulating the system described in Sec. II is based on the immersed boundary method described in [16]. The main idea is to mark with an indicator field (I) the cells where the solid is placed. Then, the mass and momentum equations can be solved, coupled with the rigid solid body equations to describe the fluid flow and the motion of the body [18]. The indicator field is defined using a heaviside step function as follows [19], and the details about the numerical treatment for updating this field at each simulation time step are reported in [16,20]. Once the indicator field is calculated, the velocity \mathbf{u} in any cell of the computational domain is obtained by

$$\mathbf{u}(\mathbf{x}) = I(\mathbf{x})\mathbf{u}_f(\mathbf{x}) + (1 - I(\mathbf{x}))\mathbf{u}_s(\mathbf{x}), \quad (1)$$

where subindexes f and s denote the fluid and solid regions, respectively. In general, for conductive fluids where electromagnetic forces appear, the magnetohydrodynamics equations must be solved. However, when working with weak electrolytes whose electrical conductivity is very small compared to that of liquid metals, induced effects are negligible. Using this approach, it is possible to solve the following mass and momentum equations for the whole domain with variable density and viscosity:

$$\nabla \cdot \mathbf{u} = 0, \quad (2)$$

$$\frac{\partial \rho \mathbf{u}}{\partial t} + \nabla \cdot \rho \mathbf{u} \mathbf{u} = -\nabla p + \nabla \cdot \mu (\nabla \mathbf{u} + \nabla^T \mathbf{u}) + I(\mathbf{j}^0 \times \mathbf{B}^0), \quad (3)$$

where p is the pressure, \mathbf{B}^0 is the magnetic field produced by the permanent magnets, \mathbf{j}^0 is the applied current density,

ρ is the mass density, and μ is the dynamic viscosity. The Lorentz force term in the momentum equations is multiplied by the indicator function since it is only applied on the fluid. The velocity computed from the momentum equations does not necessarily satisfy the rigidity condition in the solid region; therefore, the velocity field calculated by the flow solver is integrated over the solid domain for obtaining the velocity of the centroid and the angular velocity of the body as follows:

$$M_s \mathbf{u}_{sc}^{n+1} = \int (1 - I) \rho_s \mathbf{u} dV, \quad (4)$$

$$\mathbf{I}_s \Omega_z^{n+1} = \int (1 - I) \mathbf{r} \times \rho_s \mathbf{u} dV, \quad (5)$$

where M_s is the mass of the solid, \mathbf{u}_{sc} is the velocity of the centroid of the solid, \mathbf{I}_s is the moment of inertia tensor, and Ω_z is the angular velocity. Once the translational and angular velocities of the solid body are computed, the corrected velocity field in the solid region (\mathbf{u}_s) is obtained as

$$\mathbf{u}_s = \mathbf{u}_{sc} + \mathbf{r} \times \Omega_z \hat{\mathbf{k}}, \quad (6)$$

where \mathbf{r} is the position vector, that is, the distance to any point inside the solid from the center of rotation of the rigid body. Since the solid is moving through the fluid, the material properties in the domain, such as the density and viscosity depend on the position and time and must be updated at each time step. The calculation of these properties is performed through the indicator field:

$$\rho(\mathbf{x}, t) = \rho_s(1 - I(\mathbf{x}, t)) + \rho_f I(\mathbf{x}, t), \quad (7)$$

$$\mu(\mathbf{x}, t) = \mu_s(1 - I(\mathbf{x}, t)) + \mu_f I(\mathbf{x}, t). \quad (8)$$

In order to obtain a dimensionless version of the mass and momentum equations, it is convenient to introduce the following dimensionless variables:

$$\mathbf{x}^* = \frac{\mathbf{x}}{d}, \quad \mathbf{u}^* = \frac{\mathbf{u}}{u_o}, \quad \rho^* = \frac{\rho}{\rho_f}, \quad p^* = \frac{p}{\rho_f u_o^2}, \quad \mu^* = \frac{\mu}{\mu_f},$$

$$\mathbf{j}^* = \frac{\mathbf{j}}{j_0}, \quad \mathbf{B}^* = \frac{\mathbf{B}}{B_0}, \quad t^* = \frac{t}{d^2/\nu_f},$$

where d is the diameter of the plastic film, $u_o = \nu_f/d$ is the viscous characteristic velocity, and j_0 and B_0 are the magnitudes of the electric current density and magnetic field, respectively. Additionally, to take into account the friction of the fluid with the bottom of the container, we use a quasitwo-dimensional approach that involves the averaging of the equations in the z direction, normal to the free surface. Then, the averaged mass and momentum balance equations are expressed in dimensionless form as

$$\nabla \cdot \mathbf{u} = 0, \quad (9)$$

$$\frac{\partial \rho \mathbf{u}}{\partial t} + \nabla \cdot \rho \mathbf{u} \mathbf{u} = -\nabla p + \nabla \cdot \mu (\nabla \mathbf{u} + \nabla^T \mathbf{u}) - \frac{\mathbf{u}}{\tau} + QI(\mathbf{j}^0 \times \mathbf{B}^0), \quad (10)$$

where the superscript $*$ has been omitted. Further details for obtaining the nondimensional equations and the numerical implementation can be found in our previous study [16]. The

third term on the right-hand side of Eq. (10) represents the Rayleigh friction, where τ is the characteristic time scale for the damping of vorticity owing to dissipation in the viscous layers. This term appears due to the averaging of the conservation equations in the z direction [12] and the expression for computing τ is given in [16]. The flow is governed by the Lorentz force parameter, $Q = U_0/u_0$, which compares two velocity scales. The scale U_0 is defined from the balance between Lorentz and viscous forces, namely, $U_0 = j_0 B_0 d^2 / \rho_f \nu_f$ (see [12]). As in [16], the normal component of the magnetic field $B_z(x, y)$ was modeled by a Gaussian distribution that approximates very closely the distribution of a small magnetic dipole [21]. The Hartmann number is $Ha = B_0 d (\sigma / \rho \nu)^{1/2} = 0.4$. As it is lower than unity, the induced effects are negligible.

In the quasitwo-dimensional numerical model both solid bodies immersed in the fluid are characterized as circular surfaces of diameter d , which is the diameter of the plastic film that keeps the magnet afloat on the fluid. In addition to the Lorentz force parameter, the other characteristic parameter of the flow is the ratio of solid and fluid densities, ρ_s / ρ_f , which remains constant in our simulations, equal to 0.677. The numerical code considers the entire experimental domain which was discretized in a regular grid of 764×764 control volumes in the x and y directions, respectively. The time step was set to 10^{-4} for all the simulations to yield consistent results. The fluid is assumed quiescent for the initial condition and the velocity satisfies free-slip conditions at the boundaries of the container. The boundaries are away from the core flow by at least a distance of ten diameters of the plastic disks, thus their effect on the vortex formation can be considered negligible. The numerical code has been successfully validated in previous studies [16,18]. Finally, the numerical velocity fields were used to calculate the Lagrangian trajectories of passive particles in order to mimic the motion of the dyes poured on the surface of the fluid for the experimental observations.

IV. RESULTS

Figure 3 shows experimental PIV velocity fields for three different time instants of the flow produced by the rotor. Referring to the first diagram in Fig. 2, when the electric current j_x is injected, it interacts with the magnetic field of each floating magnet, producing two Lorentz forces in opposite y direction, as seen in Fig. 3(a), where the polarization of the left and right magnets is negative and positive, respectively. Each Lorentz force promotes a vortex dipole with the floating magnet at its center, as in [16]. Since the vortex dipoles are close enough for a dimensionless distance between the centroids of the magnets $D = l/d = 1.8$, the internal vortices of each dipole merge and the flow structure generated is a tripole. The jetlike flow in the central part of each vortex dipole exerts a hydrodynamic force that accelerates the floating magnets. Because the magnets are mechanically coupled, the tripole generates a torque that promotes a clockwise rotation of the system, as seen in Figs. 3(a)–3(c). When the rotor reaches a quarter full rotation, see Fig. 3(c), an electric current in the negative y direction ($-j_y$) is injected and the rotation continues cyclically.

We also performed numerical simulations following the model described in Sec. III. The flow was calculated nu-

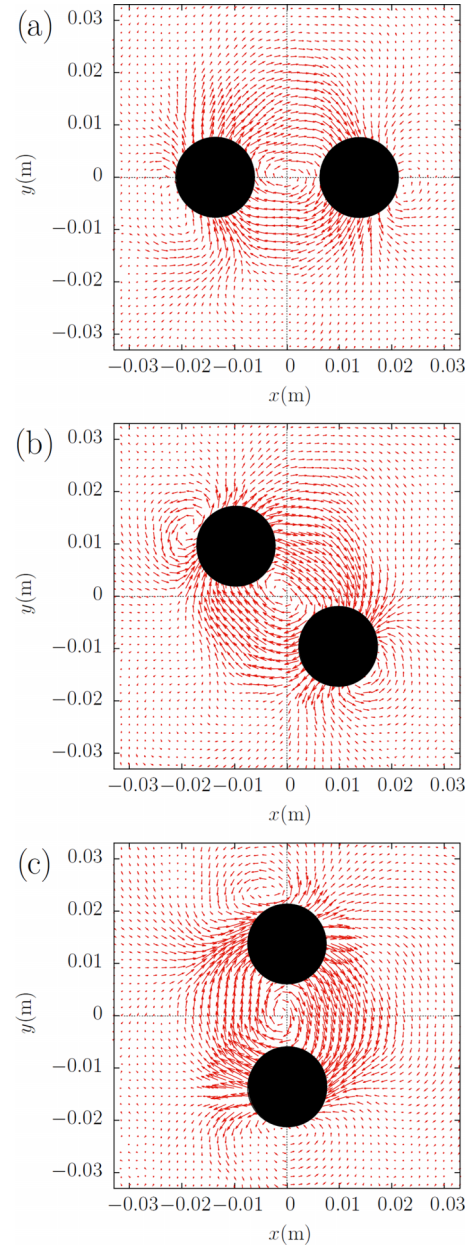


FIG. 3. Velocity fields of the tripolar flow generated by the electromagnetically driven rotor for different time instants: (a) $t = 0$, (b) $t = \pi/4$, (c) $t = \pi/2$. The black disks denote the floating magnets: $D = 1.8$, $Re = 45$. Experimental PIV observations. For velocity scale, see Fig. 4.

merically and validated with the experimental velocity fields from Fig. 3. Figure 4 shows the numerical and experimental comparison of the u component as a function of the y coordinate in the core flow at $t = 0$ [see Fig. 3(a)]. The relative error of the numerical results compared to the experimental measurements turns out to be less than 10%. It can be seen that the maximum velocity reached in the experiments was $U = 0.003$ m/s. With this characteristic velocity, the Reynolds number based on the diameter of the plastic film ($d = 0.015$ m) is $Re = Ud/\nu = 45$, which indicates a laminar flow regime. The profile depicts the change of direction in velocity of the central vortex of the tripole with zero velocity

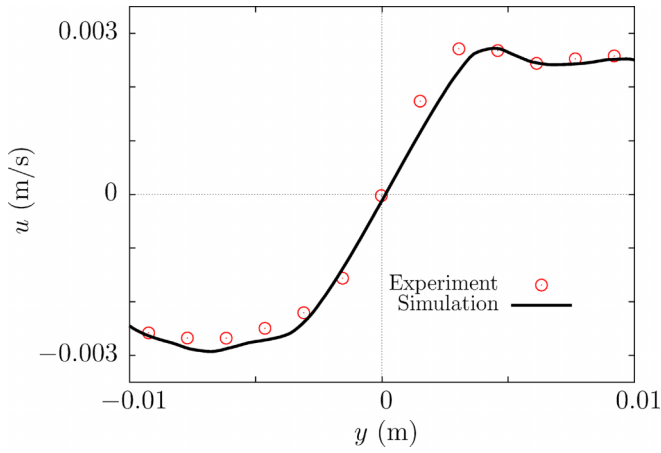


FIG. 4. Velocity component u as a function of the vertical coordinate y for $t = 0$, see vector field from Fig. 3(a).

at the origin. Even though the nonlinear effects are small, they promote an asymmetry in the profile. Additionally, the numerical simulations show that the centroid of the rotor remains almost unchanged, deviating only slightly from the rotation axis (approximately $0.01 d$) due to the symmetry in its geometry and in the applied Lorentz forces. From experimental observations, the rotor deviates approximately $0.10 d$ due to manufacturing defects and experimental errors.

Once the experimental observations of the dynamics of the flow produced by the rotor have been shown, the study of its mixing properties is undertaken. Figure 5(a) shows the initial distribution ($t = 0$) of two dye blobs with different colors, red and blue in the left and right regions, respectively. As the rotor completes one period ($t = 1 T$), it is clearly appreciated that the two dyes are mixed, that is, the stretching and folding mixing mechanism is present, see Fig. 5(b). At this stage, due to the high Péclet number ($Pe = Ud/D_m = 4.5 \times 10^5$) which implies that advection takes place for a substantial amount of time before diffusive effects act [13], the colors are not affected by the diffusive mechanism. However, after two periods of rotation ($t = 2 T$), the dye blobs have been elongated enough so that diffusive effects become present, see Figs. 5(c) and 5(d).

In order to emulate the experimental dye visualizations, a particle tracking technique was implemented. A strip of massless particles is initially located close to the rotor. The particles are colored according to their initial position in order to mimic the dye in the experiment. Even though the numerical results of the particle tracking do not take into account diffusive processes, the results compare satisfactorily with the experimental observations, as seen in the right column of Fig. 5. To explore the effect that the separation distance between the magnets has on the flow, numerical simulations were performed for four different conditions ($D = 1, 1.8, 3, 4$), considering the same electromagnetic forcing. In Fig. 6, instantaneous streamlines are shown for the flow at $t = 3 T$ for these conditions. It can be observed that two different flow structures are present. For short distances ($D = 1, 1.8$), a tripolar vortex structure is developed [Figs. 6(a) and 6(b)]. Once the distance between the magnets is sufficiently large, the two dipoles unmerge and rotate in the same direction of

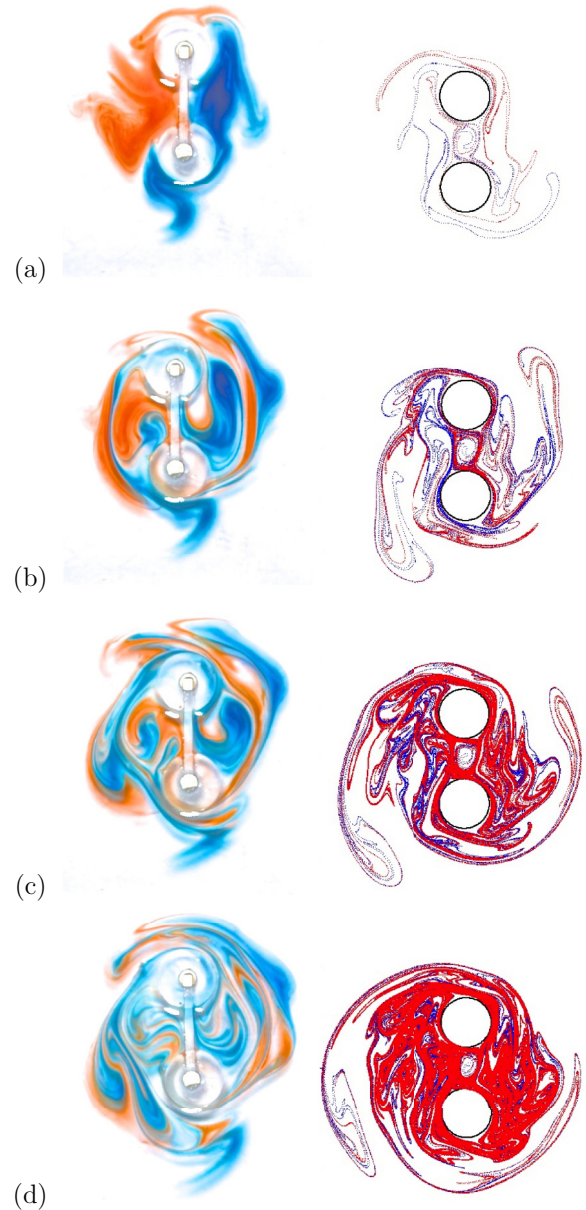


FIG. 5. Left column: Experimental visualization of the fluid mixing by the electromagnetically driven floating rotor. (a) Initial condition. (b) $t = 1 T$. (c) $t = 2 T$. (d) $t = 3 T$. $D = 1.8$, $Re = 45$, $Pe = 4.5 \times 10^5$. Right column: Numerical particle tracking visualization, the white disks denote the floating magnets.

the magnets [Figs. 6(c) and 6(d)]. As seen, each magnet produces a dipolar vortex, hence, for a small separation distance between the magnets, the dipolar structures merge to create a tripolar vortex. This produces three elliptic points, and it is well known that the surrounding flow of elliptic points interacts with the whirl generated, enhancing the mixing [22]. On the other hand, as the separation distance between the magnets increases, the tripolar vortex structure unmerges and the original dipolar vortices of each magnet are recovered. In this case, four elliptical points and one hyperbolic point appear in the flow. Since streamlines do not cross hyperbolic points, this results in an ineffective mixing mechanism [23].

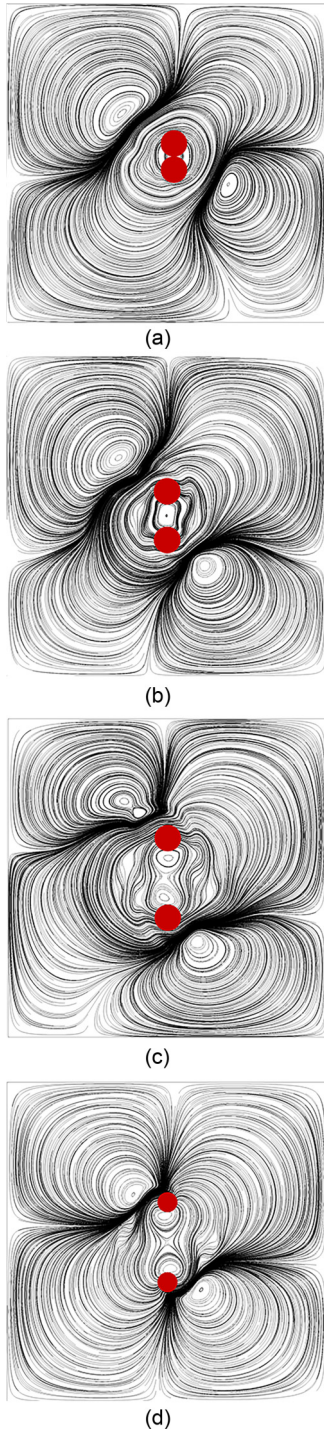


FIG. 6. Instantaneous streamlines. The red disks denote the floating magnets. (a) $D = 1$. (b) $D = 1.8$. (c) $D = 3$. (d) $D = 4$. Numerical simulations.

The corresponding angular velocities for the separation distances ($D = 1, 1.8, 3$, and 4) are, respectively, $\Omega_z = 0.34, 0.26, 0.18$, and 0.15 rad/s, whereas the related tangential velocities are $U_t = \Omega_z r = 2.6, 3.5, 4.1$, and 4.4 mm/s, with $r = l/2$. Neglecting the mass of the plastic coupling, the moment of inertia of the rotor is $I_r = 2m_s r^2$ and the angular momentum of the rotor is $L_r = I_r \Omega_z$. Thus, both L_r and I_r increase as the separation distance D also increases. Based on the tangential

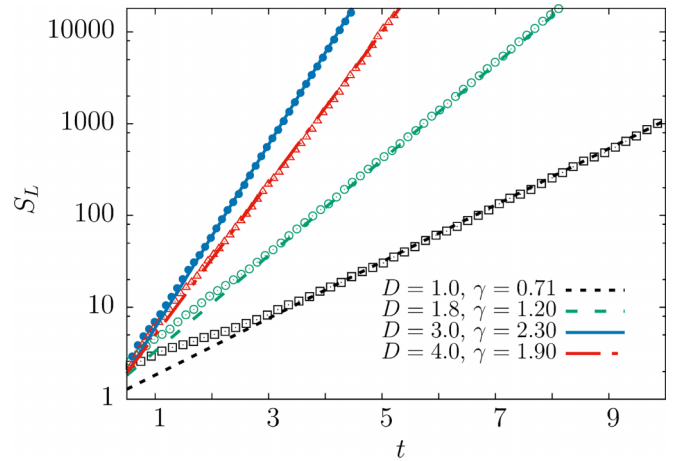


FIG. 7. Total strip length S_L as a function of time t for different D . Symbols correspond to the numerically calculated length and lines to an exponential fit using Eq. (11).

velocity of the rotor, the corresponding Reynolds number $Re_t = U_t d / \nu_f$ for Figs. 6(a)–6(d) are $Re_t = 38, 52, 60$, and 65 . The latter shows that if the electromagnetic forcing is kept constant, the rotor reaches a limit value for Re_t when the separation distance is large enough. From the dynamic point of view, the torque on the rotor is $\tau_t = r(F_L + F_v)$, where F_L and F_v denote the Lorentz and viscous forces. If these forces are balanced ($F_L \approx F_v$), the rotor will rotate at constant angular velocity. Departing from the latter assumptions, the Reynolds number can be related to the electromagnetic forcing as $Re_t = (2Q/C_D)^{1/2}$, where C_D is the drag coefficient. From a study of side-by-side cylinders [1], the drag coefficient C_D reduces 40% from $D = 1.5$ to $D = 4$. Thus, for a constant electromagnetic forcing (Q), the Reynolds number Re_t will increase as a square root of the separation distance D , which is consistent with the experimental results.

The particle tracking allows us to compute the total length of the strip S_L as it is advected by the flow. It should be noted that the detailed kinematics of the strip line are very sensitive to the location of the initial dye blob. However, the total strip length S_L grows exponentially at almost the same growth rate as when the blob is initialized in a high-stretching region. Figure 7 shows the length of the strip as a function of time for the rotor varying the distance D between the magnets. We observe that as the flow evolves, the strip stretches and folds so that its length tends to grow exponentially. The exponential growth in time of S_L by stretching and folding is indicative of chaotic mixing [23]. The length S_L is well fitted at late stages by an exponential fit:

$$S_L = S_0 e^{\gamma(t-t_0)}, \quad (11)$$

where S_0 is the initial strip length, γ corresponds to the mean stretching rate, and t_0 is the temporal delay which allows taking into account the transient stage. From Fig. 7, it can be noticed that the stretching rate increases for $D = 1, 1.8$ and reaches a maximum for $D = 3$ and then decreases for $D = 4$. This indicates that there is an optimum distance between the magnet that generates a maximum exponential growth of the length of the strip. This optimum value is close to the

transition between the tripole vortex and the two separate dipoles.

V. CONCLUDING REMARKS

The flow generated by a system of two mechanically coupled floating permanent magnets in a thin electrolyte layer was studied experimentally and theoretically. The Lorentz force promotes the motion of the magnets in opposite directions, creating a system with rotorlike behavior that stirs the fluid and eventually mixes it. Even though the rotation of the system was only presented for electric current pulses lasting 4 s at an amplitude of 700 mA, if smoother current functions and electronic feedback control were incorporated, the system would rotate for different amplitudes of electric currents and frequencies. It was possible to identify a tripolar flow structure. A time-periodic flow resulted from the interaction of two smaller structures created by the Lorentz force, namely two vortex dipoles. In this fluid-solid interaction problem, the rotor is dragged by the flow structure generated by the Lorentz force, reaching a Reynolds number of $Re = 45$. At this laminar regime, flow quasitwo-dimensionality is achieved. The numerical simulations using a Q2D model show a quantitative agreement with the PIV experimental observations. The model was based on the solution of the conservation equations coupled with an immersed boundary method to solve the dynamics of the solid body. It is important to note that the Q2D model that introduces a linear friction with the bottom wall leads to satisfactory results. Using the flow

fields calculated numerically with the Q2D model, Lagrangian particle tracking results were compared with experimental visualization using dye. The particle tracking correctly captures the main physical features of the scalar mixing promoted by the rotor. The numerical simulation predicts the stretching and folding mixing mechanisms present in the experiment very well. It was found that the mixing produced by electromagnetically driven flows is strongly influenced by the distance separating the two magnets. Furthermore, as the strip is stretched and folded, the numerical method allows to calculate the total length of the strip which was found to grow exponentially, indicating that standard chaotic mixing is achieved in the present flows. Thus, the obtained results indicate that the floating stirrer could be useful for mixing applications in low Reynolds number flows in shallow layers of electrolytes.

ACKNOWLEDGMENTS

This research was supported by Consejo Nacional de Ciencia y Tecnología (258623) and Universidad Nacional Autónoma de México (DGAPA IN107921). A.F. and S.P. thank Investigadoras e Investigadores por México program from CONACYT. A.F. also thanks Université de Tours for financial support during his sabbatical leave at Institut de Recherche sur la Biologie de l’Insecte. Finally, MEng. J. Olvera-Orozco is acknowledged for helping with the grammar and style revision of the manuscript.

-
- [1] G. J. Van-Heijst and R. C. Kloosterziel, *Nature (London)* **338**, 569 (1989).
 - [2] R. C. Kloosterziel and G. J. F. Van-Heijst, *Elsevier Oceanography Series* **50**, 609 (1989).
 - [3] C. E. Leith, *Phys. Fluids* **27**, 1388 (1984).
 - [4] B. Legras, P. Santangelo, and R. Benzi, *Europhys. Lett.* **5**, 37 (1988).
 - [5] P. Orlandi and G. J. Van-Heijst, *Fluid Dyn. Res.* **9**, 179 (1992).
 - [6] L. A. Barba and O. U. Velasco-Fuentes, in *IUTAM Symposium on Hamiltonian Dynamics, Vortex Structures, Turbulence*, 1st ed., edited by A. V. Borisov (Springer, Moscow, 2008), pp. 247–256.
 - [7] G. J. F. Van-Heijst, R. C. Kloosterziel, and C. W. Williams, *J. Fluid Mech.* **225**, 301 (1991).
 - [8] J. B. Flor, W. S. S. Govers, G. J. F. Van Heijst, and R. Van Sluis, *Appl. Sci. Res.* **51**, 405 (1993).
 - [9] R. D. Pingree and B. Lecann, *Deep Sea Research Part A. Oceanographic Research Papers* **39**, 1147 (1992).
 - [10] O. U. V. Fuentes, G. J. Van-Heijst, and N. P. Van-Lipzig, *J. Fluid Mech.* **307**, 11 (1996).
 - [11] P. J. S. A. de Sousa and J. C. F. Pereira, *J. Fluid Mech.* **634**, 41 (2009).
 - [12] A. Figueroa, F. Demiaux, S. Cuevas, and E. Ramos, *J. Fluid Mech.* **641**, 245 (2009).
 - [13] A. Figueroa, P. Meunier, S. Cuevas, E. Villiermaux, and E. Ramos, *Phys. Fluids*. **26**, 013601 (2014).
 - [14] N. T. Ouellette and J. P. Gollub, *Phys. Fluids* **20**, 064104 (2008).
 - [15] A. Figueroa, S. Cuevas, and E. Ramos, *J. Fluid Mech.* **815**, 415 (2017).
 - [16] S. Piedra, J. Román, A. Figueroa, and S. Cuevas, *Phys. Rev. Fluids* **3**, 043702 (2018).
 - [17] W. Thielicke and E. J. Stamhuis, *J. Open Res. Softw.* **2**, e30 (2014).
 - [18] D. R. Domínguez, S. Piedra, and E. Ramos, *Phys. Rev. Fluids* **6**, 064701 (2021).
 - [19] G. Tryggvason, R. Scardovelli, and S. Zaleski, *Direct Numerical Simulations of Gas-Liquid Multiphase Flows*, 1st ed. (Cambridge Press, 2011).
 - [20] S. Piedra, E. Ramos, and J. R. Herrera, *Phys. Rev. E* **91**, 063013 (2015).
 - [21] S. Cuevas, S. Smolentsev, and M. Abdou, *Phys. Rev. E* **74**, 056301 (2006).
 - [22] P. Meunier and E. Villiermaux, *J. Fluid Mech.* **476**, 213 (2003).
 - [23] J. M. Ottino, *The kinematics of Mixing: Stretching, Chaos, and Transport*, 1st ed. (Cambridge Press, 1989).